Spatio-Temporal Graph Hubness Propagation Model for Dynamic Brain Network Classification

Qi Zhu, Shengrong Li, Xiangshui Meng, Qiang Xu, Zhiqiang Zhang, Wei Shao, and Daoqiang Zhang, *Senior Member, IEEE*

***Abstract*— Dynamic brain network has the advantage over static brain network in characterizing the variation pattern of functional brain connectivity, and it has attracted increasing attention in brain disease diagnosis. However, most of the existing dynamic brain networks analysis methods rely on extracting features from independent brain networks divided by sliding windows, making them hard to reveal the high-order dynamic evolution laws of functional brain networks. Additionally, they cannot effectively extract the spatio-temporal topology features in dynamic brain networks. In this paper, we propose to use optimal transport (OT) theory to capture the topology evolution of the dynamic brain networks, and develop a multi-channel spatio-temporal graph convolutional network that collaboratively extracts the temporal and spatial features from the evolution networks. Specifically, we first adaptively evaluate the graph hubness of brain regions in the brain network of each time window, which comprehensively models information transmission among multiple brain regions. Second, the hubness propagation information across adjacent time windows is captured by optimal transport, describing high-order topology evolution of dynamic brain networks. Moreover, we develop a spatio-temporal graph convolutional network with attention mechanism to collaboratively extract the intrinsic temporal and spatial topology information from the above networks. Finally, the multi-layer perceptron is adopted for classifying the dynamic brain network. The extensive experiment on the collected epilepsy dataset and the public ADNI dataset show that our proposed method not only outperforms several state-of-the-art methods in brain disease diagnosis, but also reveals the key dynamic alterations of brain connectivities between patients and healthy controls.**

This work was supported in part by National Natural Science Foundation of China (Nos. 62076129, 62371234, 62136004, and 62272226), Natural Science Foundation of Jiangsu Province (No. BK20231438) and Key Research and Development Plan of Jiangsu Province (No. BE2022842).

Qi Zhu, Shengrong Li, Wei Shao and Daoqiang Zhang are with the College of Computer Science and Technology, Nanjing University of Aeronautics and Astronautics, Nanjing 211106, China, and also with Key Laboratory of Brain-Machine Intelligence Technology, Ministry of Education, University of Aeronautics and Astronautics, Nanjing 211106, China. E-mail: zhuqinuaa@163.com, {lisrong, shaowei20022005, dqzhang}@nuaa.edu.cn. The first two authors contributed equally to the work.

Xiangshui Meng is with the Department of Radiology, Qilu Hospital (Qingdao), Cheeloo College of Medicine, Shandong University, Qingdao 266035, China. E-mail: qdqlfsk2021@163.com.

Qiang Xu and Zhiqiang Zhang are with the Department of Medical Imaging, Nanjing Jinling Hospital, Nanjing University School of Medicine, Nanjing 210002, China. E-mail: fmrixuq@126.com, zhangzq2001@126.com.

(Corresponding authors: Daoqiang Zhang, Wei Shao, and Zhiqiang Zhang.)

***Index Terms*— dynamic brain networks, optimal transport, topology evolution, spatio-temporal feature, brain disease diagnosis**

I. Introduction

THE brain is an intricate nervous system consisting of a vast number of neurons and connectivities, which can be described as the brain network [1]. Brain network analysis has become a popular tool for diagnosing brain diseases and studying cognitive neuroscience mechanisms, as it provides a comprehensive understanding of the complex topology structure among brain regions [2]. Recent studies have shown that many neurodegenerative or psychiatric diseases, such as epilepsy [3], Alzheimer's disease [4], and major depressive disorder [5] often lead to alterations in the connection pattern of the brain network. Therefore, it is of great significance to investigate effective brain network representation and classification methods for the precise diagnosis of brain diseases and the discovery of biomarkers.

Functional magnetic resonance imaging (fMRI) has been widely used to study functional brain networks by measuring changes in blood flow and oxygenation in the brain, which can reflect the activation patterns of connectivity between different brain regions that support various cognitive and behavioral processes. In recent years, many static functional brain network (SFBN) analysis methods have been proposed in brain disease diagnosis [6], [7]. SFBN approaches aim to exploit a relatively stable network to describe the brain region correlation pattern over a period of time. Nevertheless, an increasing body of physiological evidence [8], [9] indicates that the functional brain network undergoes constant reconstruction with temporal variations, which cannot be comprehensively described by SFBN.

Different from SFBN based methods, dynamic functional brain networks (DFBNs) analysis methods treat the connection strength between brain regions as a series of values that change over time, which can reflect the time evolution tendency of the network structure. For dynamic brain networks, it is necessary to divide the functional sequence signal into several time windows and construct brain networks at each time window for analysis. For example, Jie et al. extracted temporal variability and spatial variability from each subnetwork in DFBNs, and integrated them for mild cognitive impairment (MCI) recognition [10]. Noman et al. used graph convolutional network (GCN) to encode the structure of each subnetwork in DFBNs, and then captured the dynamic changes of network

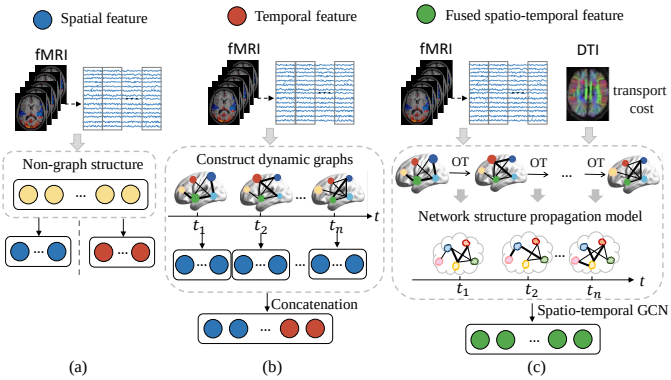

Fig. 1. Comparison of different dynamic brain networks feature extraction strategies. (a) Independently extracting temporal or spatial features from non-graph structure, (b) collaboratively extracting the spatio-temporal features by using the graph structure learning, and (c) the proposed spatio-temporal graph hubness propagation model can simultaneously reveal the network topology evolution and extract spatio-temporal graph topology features from dynamic brain networks.

topology for autism spectrum disorder classification [11]. In fact, due to the continuity of brain activity, the network structure information propagation in brain networks occurs in both spatial and temporal dimensions. Specifically, the global interaction among brain regions enables each brain region to indirectly influence its neighbors in the adjacent time window. However, the conventional dynamic brain networks methods rely solely on feature learning of independent brain networks within each time window, and they are unable to extract high-order network topology evolution information across the different time windows within the dynamic brain network.

In general, the existing works on feature extraction of dynamic brain networks can be divided into the following two categories. The first category of methods converts the brain network into a vector and then separately extracts temporal and spatial features from the dynamic network, as shown in figure 1(a). However, it is difficult to effectively decouple the highly correlated spatio-temporal topology structures in dynamic brain networks by independently extracting shallow temporal and spatial features or simply concatenating them [12]–[14]. The second category of methods directly learns the topological features from the dynamic brain networks without disrupting the graph structure information of the brain network, presented in figure 1(b), such as using graph learning [15] and tensor decomposition [16]. It is worth noting that the methods from both above two categories are hard to reveal the network structure evolution law of dynamic brain networks. Therefore, it remains a challenging task to effectively extracte the variation of spatio-temporal topology features from dynamic brain networks to improve the performance of brain disease diagnosis and biomarker identification.

In order to address the above problems, we propose a graph hubness propagation model to investigate the network topology evolution in dynamic brain networks, and develop a multi-channel spatio-temporal graph convolutional network (MCST-GCN) to extract the discriminative features from the above evolution network, as shown in figure 1(c). We first adaptively learn the graph hubness of each brain region in the brain network of each sliding window, considering the correlation among multiple brain regions. Second, we utilize optimal transport [17] to learn the dynamic evolution of graph hubness between adjacent sliding windows. Specifically, the graph hubness of the two adjacent brain networks is treated as the attribute before and after transportation, while the structural brain network from diffusion tensor imaging (DTI) is used as the transport cost. By solving the above optimal transport problem, the most economical graph hubness transport can be determined, which can be viewed as the high-order topology evolution networks (HOTENs) across the brain networks of the adjacent windows. Moreover, we design a MCST-GCN with attention mechanism to extract the discriminative features from the HOTENs. It preserves the topology information of the dynamic brain networks and effectively characterizes its dynamic evolution simultaneously in feature extraction. Finally, we feed the extracted features into a multi-layer perceptron for classification. In brief, the proposed method has the following advantages:

1) In this paper, we investigate the spatio-temporal graph structure propagation mechanism within dynamic brain networks, which effectively captures high-order topology evolution information from the brain network sequence and extracts the intrinsic spatio-temporal features for brain disease diagnosis.

2) By considering the correlation among multiple brain regions, we adaptively learn the graph hubness of the brain regions within each brain network divided by sliding window. Simultaneously, we use optimal transport to solve the graph hubness propagation model between adjacent brain networks.

3) We develop a spatio-temporal graph convolutional network with an attention mechanism for effectively extracting discriminative topology information from the obtained high-order topology evolution networks.

4) The proposed model has been evaluated on the diagnosis of epilepsy and cognitive impairment. The experimental results demonstrate that the proposed method outperforms state-of-the-art brain network analysis methods and provides spatio-temporal topological biomarkers for brain disease diagnosis.

The remainder of the paper is organized as follows: In Section II, we elaborated on the related works. Then our proposed spatio-temporal graph hubness propagation is presented in Section III. Section IV describes the materials and provides the experimental results compared with several previous brain disease diagnosis approaches. In Section V, we give a discussion of the experimental results. The summary of our work and the conclusion are presented in section VI.

II. Related Work

A. Dynamics in Brain Network

Effective modeling of brain networks is conducive to understanding the complex organizational structure and cognitive process of the brain. The dynamic model has been proven to be a powerful tool to explore the potential mechanisms of the complex nervous system [18]. Wang and Song et al. applied complex network theory to brain network analysis and mined abnormal changes in the static characteristics of brain networks, such as degree distribution, small-world attributes, etc [19], [20]. However, these approaches cannot trace the

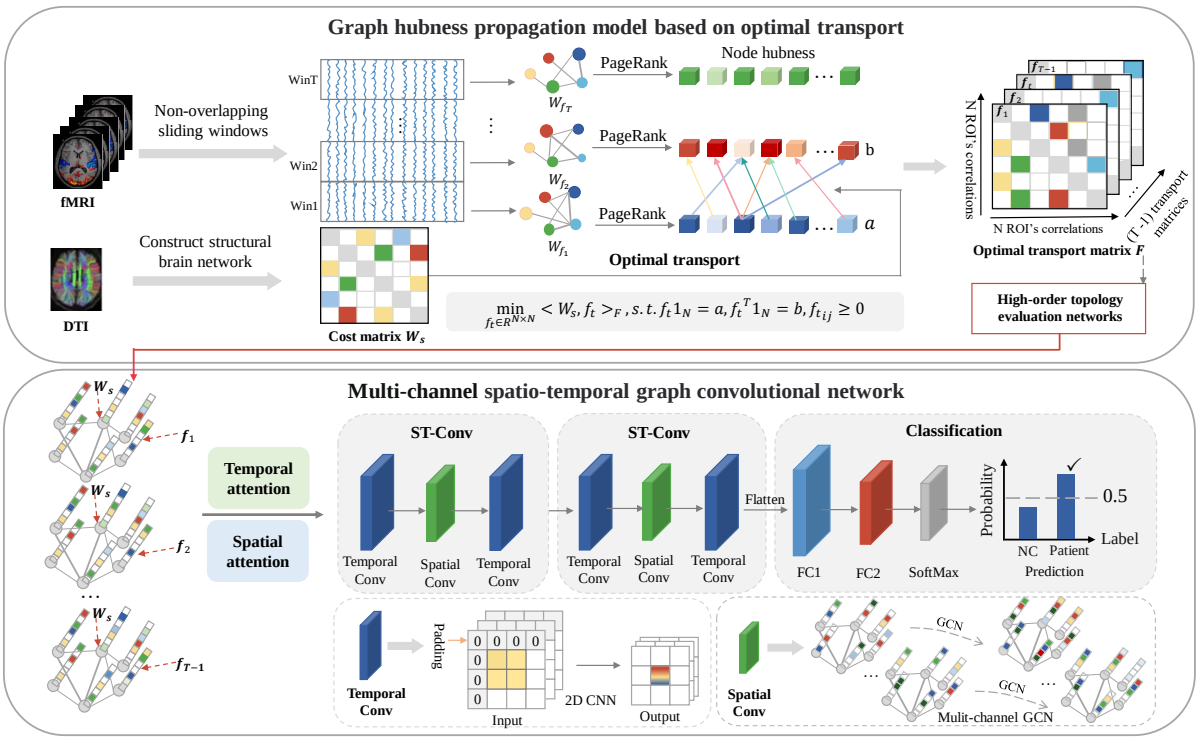

Fig. 2. The framework of the proposed spatio-temporal graph hubness propagation analysis method for brain disease diagnosis.

process of the variation of the brain network structure. The emergence of network dynamics compensates for this deficiency by adopting static features with dynamics. Watanabe et al. used fMRI to analyze the characteristics of brain dynamics in patients with autism, and found that compared with healthy people, the functional coordination pattern and over-stable neurodynamic system in the brain of patients with autism caused the occurrence of autism [21]. Zhang et al. used hidden Markov models to estimate the time-varying connectivity of functional network and capture both stationary and abrupt brain activity states [22].

However, the brain is a dynamic system of constant remodeling, showing complex forms of organization in both temporal and spatial dimensions. Some spatio-temporal feature extraction methods have been proposed to further understand the pathogenesis of brain diseases. For example, Gadgil et al. proposed to simultaneously capture the functional dependencies between brain regions and the temporal information of brain activities with spatio-temporal maps [23]. Kim et al. employed the spatio-temporal attention mechanism to learn a dynamic graph representation of brain connectivities to capture the changing characteristics of functional connectivity fluctuations over time [24]. It is worth noting that they only studied the independent changes of the brain network within each time window, which ignores the evolution process of functional brain networks. In this work, we propose the graph hubness propagation model to explore the high-order spatio-temporal interactions among adjacent subnetworks, so as to capture the dynamic evolution of brain network topology.

B. Graph Convolutional Network

Graph convolutional network is an extension of convolutional neural network (CNN) for feature extraction on irregular graphs. It has achieved superior performance in various tasks based on graph structure, such as brain network [6], traffic flow prediction [25], etc. GCN is divided into two categories, spatial domain-based graph convolution and spectral domain-based graph convolution. The spatial GCN achieves high-level graph feature extraction by continuously aggregating neighbor node information [26], and its single-layer convolution can be defined as:

$$G(A, X) = \sigma(AXW) \tag{1}$$

where A is the adjacency matrix, X is the node feature, and W is the learnable weight coefficient. σ is the activation function. Spatial GCN has been widely used in brain network. For example, Qin et al. used raw fMRI signals as features and SFBN as the adjacency matrix to extract the structural information of brain network using GCN [27]. Spectral domain graph convolution is inspired by the field of signal processing and smooths node features based on graph Fourier transform [28]. For a signal $x \in R^n$, spectral domain graph convolution can be described as follows:

$$\Theta *_G x = U\Theta(\Lambda)U^T x \tag{2}$$

where Θ is a kernel, $U \in R^{n \times n}$ is the matrix of eigenvectors of the normalized graph Laplacian. Spectral domain graph convolution has also been used in brain network analysis. For example, Ktena et al. used the Siamese spectral domain GCN to measure the similarity between a pair of brain networks, and achieved superior classification results in brain disease diagnosis [29].

III. Proposed Method

In this section, we provide a detailed introduction to the proposed method for the analysis of dynamic brain networks,

and its schematic diagram is depicted in figure 2.

A. Network Dynamics Model of Functional Brain Network

Brain region importance based on multi-region correlation: In this work, we assume that the rs-fMRI time-series data for each subject is $X = (x_1, x_2, \cdots, x_N)^T \in R^{N\times M}$, where N is the number of brain regions and M denotes the number of consecutive time series acquired. We first divide the original fMRI signal into T sub-sequences using non-overlapping sliding windows, and then use Pearson correlation coefficient (PC) [30] to construct a functional connectivity network for each sub-time series to obtain DFBN. In addition, we retain the edges with connection weights greater than a threshold α and discard the edges with connection weights less than α to eliminate weak connectivities in the network. Next, we use PageRank to measure the network hubness to derive the importance of each node based on the graph structure in the subnetwork. The hubness of the node u depends on the number and hubness of its neighbors, which can be formulated as [31]:

$$h(u)_{i+1} = \sum_{v\in B(u)} \frac{h(v)_i}{D_v} \tag{3}$$

where $B(u)$ represents the set of the nodes connected to node u. D_v denotes the degree of node v, which is used to average the contribution of neighboring nodes v to the hubness of the node u. In addtion, $h(v)_i$ is the hubness scores of nodes v at the i^{th} iteration, and the initial hubness of each node is set to $\frac{1}{N}$ at iteration 0, where N denotes the number of nodes in the graph. We need to iterate Eq. (3) until it converges to get the hubness scores of nodes. Eq. (3) shows that the importance of nodes mainly depends on the following two conditions. On one hand, a brain region is more important if it has more neighboring nodes. On the other hand, if the neighboring nodes of a brain region are more important, the brain region itself is considered more important.

By substituting each brain region into Eq. (3), we can get the hubness distribution h_t ($t \in \{1, 2, \cdots, T\}$) of all brain regions for each subnetwork in DFBNs. Therefore, the hubness of all subnetworks of the dynamic brain networks are represented by $H = [h_1, h_2, \cdots, h_T] \in \mathbb{R}^{N\times T}$.

Hubness propagation in functional brain network with optimal transport: In order to capture the dynamic evolution of brain network spatial topology, we construct a node hubness propagation model across adjacent subnetworks by optimal transport. Specifically, we take the node hubness distribution of the $t-1^{th}$ subnetwork as the source domain, the hubness distribution of the t^{th} subnetwork as the target domain, and use optimal transport to realize the propagation process of the hubness of brain regions from the source domain to the target domain. It simulates the global interaction among brain regions, and captures the topology evolution of the DFBNs. The transport process is shown in figure 3.

Kantorovich discrete optimal transport [17] allows each brain region and multiple other brain regions in the brain network to transmit hubness, and this many-to-many transport strategy is consistent with the global high-order interaction between brain regions. The purpose of optimal transport is

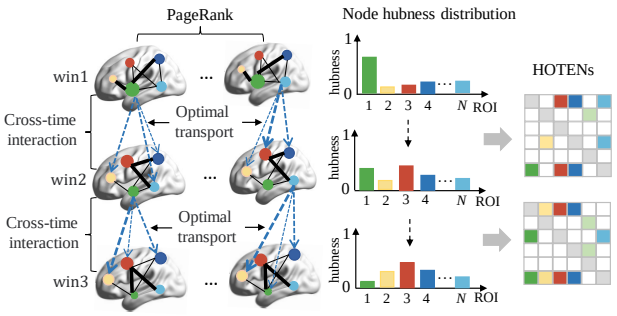

Fig. 3. Schematic diagram of the node hubness propagation process of brain regions in adjacent brain networks. The size of the nodes corresponds to the node hubness of the brain region, and the node hubness propagation of brain regions in adjacent brain networks is represented by blue dashed lines, where thicker lines indicate more transmitted hubness and stronger correlation.

to find the optimal transport matrix f_{t-1} between the two node hubness distributions of the $t-1^{th}$ and t^{th} subnetwork. Considering that the structural brain network provides a physiological basis for functional brain network, we refer to the structural brain network as the transport cost matrix W_s. The hubness transport between adjacent subnetworks can be learned by:

$$\begin{aligned} &\min_{f_{t-1}\in R^{N\times N}} \langle W_s, f_{t-1}\rangle_F, \\ &s.t.\ f_{t-1}\mathbf{1}_N = h_{t-1},\ {f_{t-1}}^T\mathbf{1}_N = h_t, \\ &f_{t-1}\mathbf{1}_N = \Sigma_j f_{t-1_{ij}},\ {f_{t-1}}^T\mathbf{1}_N = \Sigma_i f_{t-1_{ij}} \end{aligned} \tag{4}$$

where $\langle\cdot,\cdot\rangle_F$ denotes the Frobenius inner product of matrices, $\langle W_s, f_{t-1}\rangle_F = \sum_i\sum_j W_{s_{ij}} f_{t-1_{ij}}$, $W_{s_{ij}}$ and $f_{t-1_{ij}}$ denote the transport cost and the hubness movement from $h_{t-1}(i)$ to $h_t(j)$, respectively, and 1_N is an N-dimensional vector taking all values of 1.

Next, we use the Sinkhorn [32] algorithm to solve the optimal transport problem, Specifically, the entropy regularization function is first introduced as follows :

$$H\big(f_{t-1}\big) = -\sum_{i,j} f_{t-1_{ij}}(log\big(f_{t-1_{ij}}\big) - 1) \tag{5}$$

The entropy regularization function is used to regularize Eq. (4), so that the objective function of the entropy-regularized optimal transport plan is:

$$\begin{aligned} &\min_{f_{t-1}\in R^{N\times N}} \langle W_s,\ f_{t-1}\rangle_F - \varepsilon H\big(f_{t-1}\big), \\ &s.t. f_{t-1}\mathbf{1}_N = h_{t-1},\ {f_{t-1}}^T\mathbf{1}_N = h_t \end{aligned} \tag{6}$$

where ε is a regularization factor. Next, the optimal value is calculated using the matrix deflation method. Two nonnegative deflation vectors u, v are introduced as unique product factors, and the optimal mass transport scheme is expressed as:

$$f_{t-1_{ij}} = diag(u_i)K_{ij}diag(v_j) \tag{7}$$

where $K_{ij} = exp\ (-W_{s_{ij}}/\varepsilon)$. The total hubness of the brain regions remains constant during transport, so K satisfies:

$$u \circ (Kv) = h_{t-1},\ \nu \circ (K^T u) = h_t \tag{8}$$

where $\circ$ denotes the product corresponding to each element in a matrix or vector. To solve the problem, we solve for u and

v using the iterative method shown in Eq. (9), we repeat this process iteratively until convergence is achieved.

$$u^{\ell+1} = \frac{h_{t-1}}{Kv^{\ell}},\ v^{\ell+1} = \frac{h_t}{K^T u^{\ell+1}},\ v^0 = 1_N \tag{9}$$

When both equations are satisfied simultaneously, we then take u and v into Eq. (7) to solve for the optimal transport matrix. Finally, we denote the optimal transport matrix f_{t-1} computed between the $t-1^{th}$ and t^{th} subnetwork as the high-order topology evolution networks. Thus, HOTENs can be denoted as $F = (f_1, f_2, \cdots, f_{T-1})^T \in R^{(T-1)\times N\times N}$.

B. Multi-Channel Spatio-Temporal Graph Convolutional Network

We design a multi-channel spatio-temporal graph convolutional network to collaboratively capture high-order spatio-temporal features in HOTENs. Specifically, we first use the spatio-temporal attention mechanism to automatically focus on the valuable temporal and spatial information in HOTENs. Then, multi-channel graph convolution is used to extract the topological structure information in the network. Considering that HOTENs can comprehensively represent temporal and spatial features, we use 2D CNN, which is better at capturing contextual relationships, to extract the temporal information.

Spatial attention module: In the spatial dimension, different brain regions and connections have different effects on brain diseases. To be able to automatically extract valuable spatial dynamic information, we exploit spatial attention $P \in R^{N\times N}$, defined as follows:

$$P = softmax(V_p \cdot sigmoid((F^T Z_1)Z_2(Z_3 F^T)^T + b_p)) \tag{10}$$

where $V_p, b_p \in R^{N\times N}$, $Z_1 \in R^{T-1}$, $Z_2 \in R^{N\times(T-1)}$, and $Z_3 \in R^N$ all denote learnable parameters. $\cdot$ represents the multiplication of the corresponding elements of the two matrices. When performing the graph convolution operation, we first use the spatial attention matrix P to focus on the valuable spatial information. For ease of understanding, we provide a description about the output dimensions of some matrix multiplications in Eq. (10). Specifically, $F^T Z_1 \in R^{N\times N}$, $(F^T Z_1)Z_2 \in R^{N\times(T-1)}$, $(Z_3 F^T)^T \in R^{(T-1)\times N}$, $(F^T Z_1)Z_2(Z_3 F^T)^T \in R^{N\times N}$, and $V_p \cdot sigmoid((F^T Z_1)Z_2(Z_3 F^T)^T + b_p)) \in R^{N\times N}$.

Temporal attention module: In the temporal dimension, correlations exist between adjacent brain networks, and the correlations vary with time. Therefore, the temporal attention mechanism is used to capture important temporal information between dynamic brain networks. The temporal attention $Q \in R^{(T-1)\times(T-1)}$ is defined as follows:

$$Q = softmax(V_q \cdot sigmoid((FM_1)M_2(M_3 F^T) + b_q)) \tag{11}$$

where $V_q, b_q \in R^{(T-1)\times(T-1)}$, $M_1, M_3 \in R^N$, $M_2 \in R^{N\times N}$ denote the learnable parameters. We use the temporal attention matrix Q to caputre important temporal information: $\hat{F} = (\hat{f}_1, \hat{f}_2, \cdots, \hat{f}_{T-1}) = (f_1, f_2, \cdots, f_{T-1})Q$. We also provide a description about the output dimensions of some matrix multiplications in Eq. (11). Specifically, $FM_1 \in R^{(T-1)\times N}$, $(FM_1)M_2 \in R^{(T-1)\times N}$, $M_3 F^T \in R^{N\times(T-1)}$, $(FM_1)M_2(M_3 F^T) \in R^{(T-1)\times(T-1)}$, and $V_q \cdot sigmoid((FM_1)M_2(M_3 F^T) + b_q) \in R^{(T-1)\times(T-1)}$.

Spatio-temporal convolutional module: As shown in figure 2, this module is designed as a sandwich architecture to quickly aggregate spatio-temporal information [25]. Since the brain's physical connections change over time, we use 2D CNN to capture the temporal information transfer across time windows. In spectral GCN, the structural brain network provides the adjacency matrix A, and HOTENs are used as node features to extract the topology information in the brain network. The Chebyshev graph convolution [28] using a polynomial of order $K-1$ is defined as:

$$g_\Theta *_G x = g_\Theta(L)x = \sum_k^{K-1} \Theta_k T_k(\tilde{L})x \tag{12}$$

where g_Θ denotes the convolution kernel, $*_G$ is the graph convolution operation, $\Theta \in R^K$ represents the convolution kernel the Chebyshev coefficient vector, and x is the node feature. $L = D - A$ represents the Laplace matrix, where $D \in R^{N\times N}$ denotes the degree matrix. $\tilde{L} = \frac{2}{\lambda_{\max}}L - I_N$, where $\lambda_{\max}$ is the maximum eigenvalue of the Laplace matrix, and I_N is the identity matrix. $T_k(x) = 2xT_{k-1}(x) - T_{k-2}(x)$ denotes the recursive Chebyshev polynomial, where $T_0(x) = 1$, and $T_1(x) = x$. By using the approximate expansion of the Chebyshev polynomial, the feature of neighboring 0 to $K-1$ order neighbors centered at each node is extracted.

In this work, we generalize the above definition of spectral graph convolution to node features with multiple channels. The input for layer l^{th} is $\hat{F}^{(l-1)} = \left(\hat{f}_1, \hat{f}_2, \cdots, \hat{f}_{T-1}\right)^{(l-1)} \in R^{N\times C_{l-1}\times(T-1)}$, where c_{l-1} denotes the number of channels per node, i.e., $l = 1$, $C_0 = N$, and T denotes the number of sliding windows. For each $\hat{f}_i$, we use a filter c_l on the obtained topology evaluation networks $\hat{f}_i$ to acquire $g_\Theta *_G \hat{f}_i$, where $\Theta = (\Theta_1, \Theta_2, ..., \Theta_{C_l}) \in R^{K\times C_{l-1}\times C_l}$ are the parameters of the convolution kernel. Hence, the hubness from 0 to $K-1$ order neighbors is aggregated to each node. For the output $\hat{F}^{(l)}$ of l^{th} layer of the l^{th} spatio-temporal convolutional block, it can be calculated as follows:

$$\hat{F}^{(l)} = CNN(Relu(g_\Theta *_G (CNN(\hat{F}^{(l-1)})))) \tag{13}$$

Finally, two fully connected layers are used to learn the mapping relationship between dynamic features and disease progression prediction. Algorithm 1 provides a summary of the proposed method in this work.

IV. Experiment

A. Materials

1) Data Acquisition: In this work, we conduct experiments on the epilepsy dataset and the Alzheimer's Disease Neuroimaging Initiative (ADNI) dataset (http://adni.loni.usc.edu/). The datasets are described as follows:

Epilepsy: The rs-fMRI and DTI data used in the experiment were collected from Jinling Hospital, Nanjing University School of Medicine. The dataset contains 306 subjects, including 114 normal controls (NC), 103 patients with frontal lobe epilepsy (FLE), and 89 patients with temporal lobe epilepsy

Algorithm 1 The Algorithm of the Proposed Method.

Input: fMRI data, DTI data, ground truth label Y, hyperparameters α, ε, the number of sliding window T, $v^0 = 1_N$, max_epoch;

Output: model parameter set;

Construct DFBNs $\{W_{f_t}\}_{t=1}^{T}$ and structural network W_s;
Set a threshold α for $\{W_{f_t}\}_{t=1}^{T}$;
Calculate the node hubness $\{h_t\}_{t=1}^{T}$ by Eq. (3);
for $t = 1, 2, 3, \cdots, T$ **do**
    Calculate the OT matrix f_{t-1} between h_{t-1} and h_t by Eq. (4);
    Use Sinkhorn to solve OT matrix f_{t-1} by Eq. (5);
    Calculate the element-wise exponential K of W_s: $K_{ij} = exp\ (-W_{s_{ij}}/\varepsilon)$;
    while not converged **do**
        $u^{\ell+1} = \frac{h_{t-1}}{Kv^{\ell}}$, $v^{\ell+1} = \frac{h_t}{K^T u^{\ell+1}}$;
    end while
    $f_{t-1} = diag(u)Kdiag(v)$;
end for
while $epoch < max\_epoch$ **do**
    Obtain valuable spatio-temporal information by Eq. (10) and Eq.(11);
    Extract spatio-temporal feature of $\{f_t\}_{t=1}^{T-1}$ by Eq. (13);
    Calculate the cross-entropy loss of the predicted label and the Y;
    Back-propagate cross-entropy loss to update model parameters;
end while
return model parameter set;

(TLE). The equipment for collecting data is the Siemens Trio 3T scanner. The scan parameters of rs-fMRI are as follows: repetition time = 2000ms, echo time = 30 ms, flip angle = 90°, and voxel size $= 3.75 \times 3.75 \times 3.75 mm^3$. DTI scan parameters are repetition time = 6100 ms, echo time = 93 ms, flip angle = 90°, and voxel size $= 0.94 \times 0.94 \times 3 mm^3$, respectively.

ADNI: We collected 226 samples from ADNI2 and ADNI3, each containing fMRI and DTI modalities. The ADNI dataset contains 82 normal controls (NC), 76 patients with significant memory concern (SMC), and 69 patients with early mild cognitive impairment (EMCI). Among them, the NC group contained 40 males and 42 females with an average age of 74.31. The SMC group consisted of 50 males and 29 females with a mean age of 77.24, and the EMCI group consisted of 37 males and 32 females with a mean age of 74.77.

2) Preprocessing: Epilepsy and ADNI datasets are preprocessed in the same way. Specifically, We use the SPM8 as implemented in the DPARSF toolbox for all rs-fMRI data preprocessing. To correct and realign the initial images, the serialized data is split into several pieces and then adjusted to the EPI template. We utilize detrending to reduce the influence of head motion and the interference from CSF and white matter. After the preprocessing, the Automated Anatomical Labeling (AAL) atlas is used to divide rs-fMRI of epilepsy into 90 ROIs with 240 time points, and the AAL atlas is used to divide rs-fMRI of ADNI into 90 ROIs with 197 time points. In addition, PANDA is applied to the preprocessing of DTI data. The FSL toolbox is used to correct DTI distortion, and TrackVis is used to generate fiber images and to specify anatomical regions using AAL criteria based on the subject's T1 images. Finally, the number of fibers can be considered as a measure of the structural connection.

B. Comparison Methods

To verify the validity of the proposed method, we compared it with several brain network analysis methods, including 10 brain network construction methods and 14 feature extraction methods. The following brain network construction methods compared, including static brain network methods: sparse low-rank (SLR) [33], PC [30], functional brain network generation (FBNetGen) [34], effective functional brain network (EFBN) [35] and topographical profile similarity-based high-order functional connectivity (tHOFC) [36], and dynamic brain networks methods: dynamic functional connectivity (DFC) [37], subtractive dynamic functional brain networks obtained by subtracting adjacent subnetworks (SDFBNs), dynamic high-order functional connectivity (DHOFC) [38], high-order dynamic functional connectivity networks (Ho-D-FCNs) [39] and hybrid high-order functional connectivity networks (HybridNet) [40]. In the compared feature extraction methods, DTI-based methods include convolutional neural networks for brain networks (BrainNetCNN) [41], graph convolutional neural networks (GCNN) [42] and multi-task graph structure learning framework based on node clustering (MNC-Net) [43]. FMRI-based methods include graph sample and aggregate (GraphSAGE) [26], self-attention graph pooling (SAGPool) [44], complementary graph representation learning (CGRL) [45], dynamic functional and effective connectivity fusion (FE-STGNN) [46] and spatio-temporal functional MRI (ST-fMRI) [23]. DTI&fMRI-based methods include graph attention networks (GAT) [47], adaptive multi-channel graph convolutional networks (AM-GCN) [48], multi-modal graph convolutional network (M-GCN) [49], Siamese community-preserving graph convolutional network (SCP-GCN) [50], spatio-temporal graph convolution network (ST-GCN) [51] and spatio-temporal attention graph isomorphism network (STAGIN) [24]. In particular, for the multi-modal comparison methods with graph learning, we use DTI as the adjacency matrix and fMRI as node features. Table I lists the features and classifiers used by the proposed method and the comparison methods.

C. Implementation

The proposed method is implemented using Python based on Pytorch, and the model is trained on a single GPU (NVIDIA GeForce RTX 3080). We optimize the proposed method via the Adam algorithm, with the learning rate of 5e-3, and weigh decay is set to 1e-3. The number of epochs is set to 300, and the batch-size is set to 20. We use one layer of MCST-GCN for spatio-temporal feature extraction. In the temporal convolution block, the size of each convolution kernel is 3*3 and the stride is 1. In the spatial convolution block, the size of the graph convolution kernel is 45, and the

TABLE I
FEATURE EXTRACTORS AND CLASSIFIERS USED BY THE PROPOSED METHOD AND THE COMPARISON METHODS.

Method	Feature	Classifier
SLR [33] PC [30]	SFBN	SVM
FBNetGen [34] GraphSAGE [26] SAGPool [44]	SFBN	MLP
EFBN [35] tHOFC [36]	High-order SFBN	SVM
DFC [37] SDFBNs CGRL [45] FE-STGNN [46]	DFBNs	SVM
DHOFC [38] Ho-D-FCNs [39] HybridNet [40]	High-order DFBNs	SVM
BrainnetCNN [41] GCNN [42] MNC-Net [43]	Structural network	MLP
ST-fMRI [23]	Spatio-temporal feature of DFBNs	MLP
GAT [47] AM-GCN [48] M-GCN [49] SCP-GCN [50]	Complementary feature of structural network and SFBN	MLP
ST-GCN [51] STAGIN [24]	Spatio-temporal feature of DFBNs and structural network	MLP
Ours	Spatio-temporal feature of HOTENs and structural network	MLP

order of the Chebyshev polynomial is set to 3. Based on the output of MCST-GCN, we first use the flatten operation to pull the features into one-dimensional vectors, and then apply the multi-layer perceptron to predict the category for each subject. The number of neurons in the two fully connected layers is 1024, 256, respectively, where softmax is used as the activation function of the last fully connected layer. Our code is available at: https://github.com/xbrainnet/OT-MCSTGCN.

In this paper, we evaluate the performance of different algorithms on epilepsy and ADNI datasets by 10-fold cross validation. Specifically, we divide the whole dataset into ten mutually exclusive subsets, nine of which are used as training set and the remaining subset is used as for testing. We divided 20% of the samples in the training set into the validation set, and the best performing model on the validation set is selected for testing. The experiment is repeated for ten times, and the average results of these ten experiments are reported.

In the experiments, we employ grid search to determine the optimal combination of hyperparameters, including the number of sliding windows T, the threshold α, and the regularization coefficient ε. Specifically, in dynamic brain networks construction, to avoid the arbitrariness of the number of sliding windows and threshold α, we set the numbers of sliding windows located in $\{2, 3, 4, 5, 6, 7, 8, 9, 10\}$, while α ranges from 0.1 to 0.9 with a step size of 0.05. In solving the optimal transport, ε in Eq. (6) is selected in the range of {1e-4, 1e-3, 1e-2, 1e-1, 1}. With each hyperparameter combination, we construct the dynamic brain network by optimal transport and then train MCST-GCN on the training set in 10-fold cross validation. The classification accuracy on the validation set is used to evaluate the model performance under the hyperparameter combination. In addition, the parameters of the proposed MCST-GCN are determined by 10-fold cross validation. In the 10-fold cross validation, we also use the validation set to determine the parameters of the proposed MCST-GCN, and the parameters that perform best on the validation set are selected. The training set, validation set and test set are independent of each other. We also follow the same parameter determination principles for all the comparison methods. We conduct experiments under four classification tasks on epilepsy dataset: NC vs TLE&FLE, NC vs. TLE, NC vs. FLE, and TLE vs. FLE. For the ADNI dataset, we conduct experiments under four classification tasks NC vs. SMC&EMCI, NC vs. SMC, NC vs. EMCI, and SMC vs. EMCI. The performance of the classification is evaluated by accuracy (ACC), F-Measure (F1), and the area under the receiver operation characteristic curve (AUC).

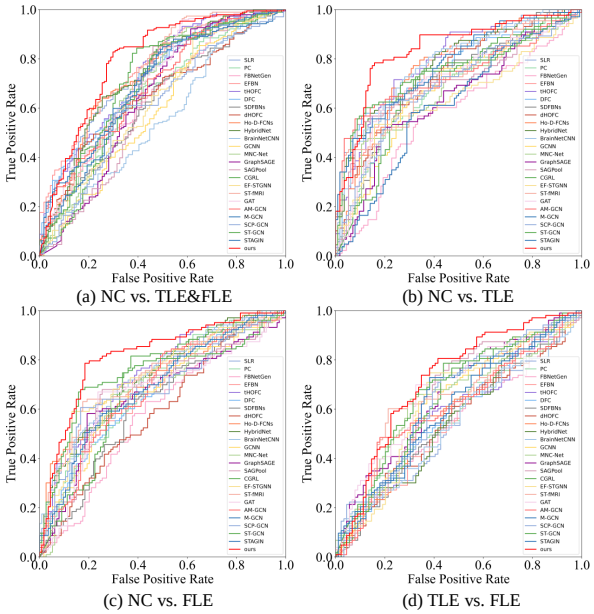

Fig. 4. ROC curves of the proposed method and comparison algorithms for brain disease diagnosis on different tasks.

D. Classification Performance

Table II and Table III show the classification results of our proposed method and the comparison methods on two datasets. It can be seen from the table that the accuracies of the proposed method on the four classification tasks on the epilepsy dataset are 81.05%, 80.21%, 81.56% and 71.92%, respectively, the accuracies of the proposed method on the four classification tasks on the ADNI dataset are 94.75%, 91.71%, 94.67% and 90.52%, respectively. The proposed method performs the best among all comparison methods. In addition, we plotted the ROC curve of the proposed method and all other comparison methods in each classification task on epilepsy dataset, as shown in figure 4. As can be seen in figure 4, the ROC curve of our method is located at the top left of all the comparison methods and has the highest AUC value. These experimental results demonstrate the effectiveness of our proposed method in identifying epilepsy and its subtypes. The reason why our method can perform better is that we do not only capture the dynamic evolution information of the brain network, but also

collaboratively extract discriminative spatio-temporal features. Compared with the static brain networks, such as SLR and PC, which lose the dynamic characteristics, and the dynamic brain networks such as DFC and DHOFC, which ignore the high-order information propagation process of the brain network, our method based on optimal transport can simulate the dynamic evolution of brain regions across time windows. In addition, compared with other feature extraction methods such as BrainNetCNN, SAGPool, ST-GCN, which lose discriminative spatio-temporal features, our MCST-GCN with spatio-temporal attention mechanism can automatically focus on more valuable spatio-temporal information. Therefore, our method can achieve promising classification performance in brain network classification.

V. DISCUSSION

A. Analysis of Parameter Sensitivity

In the proposed method, there are two hyperparameters, including the brain network threshold α and the regularization coefficient ε. We discuss the diagnostic performance of brain diseases under different parameter combinations. In the experiment, we employ grid search to investigate whether these two parameters are sensitive to the experimental results. Specifically, we set α to range from 0.1 to 0.9 with a step size of 0.05, and set ε in the range of {1e-4, 1e-3, 1e-2, 1e-1, 1}. The experimental results are presented in figure 5. It can be found from figure 5 that when α is too small or too large, it will produce relatively low classification results, which is because a small threshold will lead to a large amount of redundant information in the preserved connectivities, and a large threshold will make the brain network very sparse and lead to a reduction in topology information in the obtained brain network. However, when the threshold is between 0.4 and 0.75, no matter what the value of the other parameter is, the results will not be greatly affected. In general, the proposed method is insensitive to these two hyperparameters.

B. Visualization of Dynamic Brain Networks

To intuitively demonstrate the ability of the construction methods on different dynamic brain networks in describing the dynamic evolution and high-order interactions of brain topology, we visualize HOTENs and the other three dynamic brain networks in figure 6. As can be seen from figure 6, DFBNs and HO-D-FCNs only focus on the topological structure information within each time window and do not extract the relationship between windows. Although SDFBNs can capture the local changes in independent connections between brain regions to some extent, it is crucial to acknowledge that the connections among real brain regions involve intricate high-order relationships. Disregarding the global evolution of the high-order brain network information may lead to a potential decrease in classification accuracy. The proposed HOTENs can capture the spatio-temporal connectivity patterns in the dynamic brain network. Figure 6(d) shows the hubness propagation between brain networks from the adjacent time windows. Specifically, the horizontal blue line indicates that less hubness is transmitted from the corresponding brain region to other brain regions, and the vertical blue line indicates that the corresponding brain region receives less hubness from other brain regions.

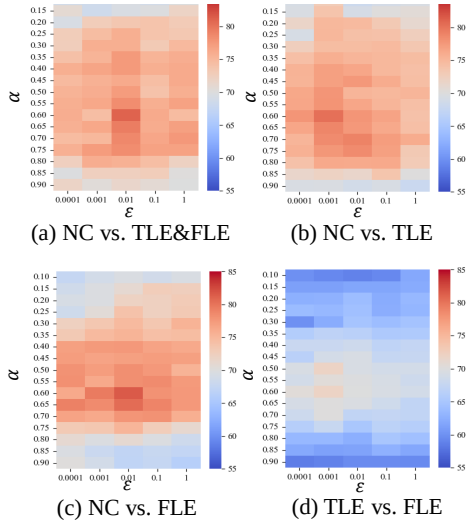

Fig. 5. The influence of hyperparameters α and ε on different classification tasks.

C. Ablation Study

To verify the effectiveness of dynamic networks, optimal transport, and MCST-GCN in our proposed method, we conduct ablation experiments on two datasets and present experiment results in Table IV. In Table IV, we use ✓to indicate that this corresponding component is used, otherwise it is not used. Compared with Ours5, Ours6 and Ours7, we can find that discarding any of the dynamic network, optimal transport or MCST-GCN components will reduce the accuracy of brain disease diagnosis. Comparing Ours2, Ours3, Ours4 with Ours5, Ours6, Ours7, we can find that discarding any two of the three components will cause a decrease in accuracy, which further indicates that these components can effectively improve the accuracy of brain diseases. For ours5, the experimental results obtained by combining dynamic network and optimal transport to construct brain network for classification are significantly better than the results of other ablation experiments, which indicates that our HOTENs constructed

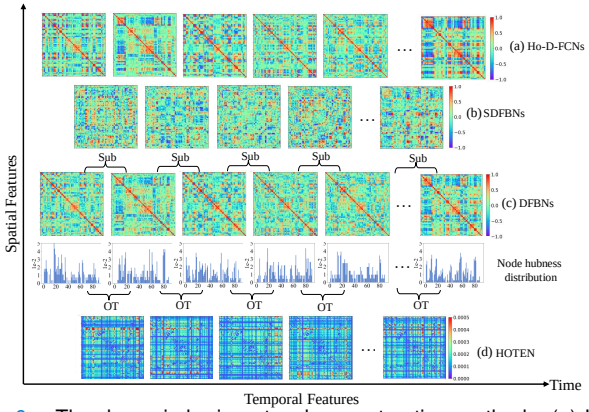

Fig. 6. The dynamic brain networks construction methods: (a) Ho-D-FCNs constructed with correlation's correlation strategy, (b) SDFBNs obtained by subtraction (Sub) of adjacent subnetworks, (c) DFBNs, and (d) The proposed HOTENs constructed with OT.

TABLE II
THE CLASSIFICATION RESULT OF THE PROPOSED METHOD AND DIFFERENT BRAIN NETWORK CONSTRUCTION METHODS (%)

Dataset	Brain network construction	Method	NC vs. TLE&FLE			NC vs. TLE			NC vs. FLE			TLE vs. FLE		
			ACC	F1	AUC	ACC	F1	AUC	ACC	F1	AUC	ACC	F1	AUC
Epilepsy	Static	SLR [33]	69.32	77.48	74.17	66.40	54.95	71.71	63.66	59.26	70.05	53.68	69.22	54.84
		PC [30]	64.05	76.96	76.72	64.36	58.49	70.42	60.84	52.18	70.19	55.32	58.41	58.07
		FBNetGen [34]	69.26	80.01	65.13	66.88	50.63	57.76	61.36	52.08	54.65	58.89	66.03	51.24
		EFBN [35]	69.20	75.72	73.80	68.36	55.59	76.93	62.19	59.40	70.55	56.34	68.50	60.73
		tHOFC [36]	69.20	74.71	73.69	71.26	65.23	77.65	66.30	63.30	74.20	60.00	59.52	56.92
	Dynamic	DFC [37]	69.97	78.22	73.18	71.80	63.23	76.65	62.12	56.79	65.86	56.37	60.68	60.22
		SDFBNs	69.97	75.72	65.52	70.83	66.95	68.90	63.05	59.79	62.66	57.79	61.24	52.67
		DHOFC [38]	74.42	80.38	67.33	75.00	73.68	75.00	65.00	53.33	59.52	56.22	62.25	58.31
		Ho-D-FCNs [39]	72.90	79.55	73.65	71.69	65.80	77.55	64.52	61.76	73.33	57.76	61.82	59.83
		HybridNet [40]	72.26	79.12	73.40	72.69	61.86	76.69	67.66	65.63	73.53	55.74	59.56	57.11
		Ours	**81.05**	**85.54**	**80.79**	**80.21**	**76.73**	**78.14**	**81.56**	**73.70**	**81.27**	**71.92**	**71.27**	**69.51**
Dataset	Brain network construction	Method	NC vs. SMC&EMCI			NC vs. SMC			NC vs. EMCI			SMC vs. EMCI		
			ACC	F1	AUC	ACC	F1	AUC	ACC	F1	AUC	ACC	F1	AUC
ADNI	Static	SLR [33]	77.43	82.21	87.61	81.62	76.49	86.45	78.00	70.44	86.06	56.76	59.96	62.06
		PC [30]	83.60	86.38	88.41	80.29	77.22	88.66	80.67	76.74	89.84	65.14	66.62	64.23
		FBNetGen [34]	81.84	87.37	85.55	80.83	72.17	76.62	78.67	72.68	79.37	70.76	70.48	58.32
		EFBN [35]	81.82	87.50	88.54	81.25	82.35	82.54	80.00	72.73	75.93	71.43	71.43	85.71
		tHOFC [36]	76.05	81.73	82.84	81.00	76.88	83.61	70.60	64.16	75.08	59.48	60.40	60.67
	Dynamic	DFC [37]	75.28	80.68	82.52	82.92	80.17	90.58	70.66	64.48	82.54	56.95	60.28	63.79
		SDFBN	78.77	82.38	84.44	75.25	74.84	81.50	73.33	70.62	79.75	68.90	71.73	65.50
		DHOFC [38]	73.08	77.73	78.44	73.42	69.23	78.91	70.67	64.73	76.58	64.29	61.54	81.25
		Ho-D-FCNs [39]	73.97	80.00	82.06	76.71	67.44	84.70	69.33	59.87	80.95	59.95	55.95	67.20
		HybridNet [40]	77.89	79.62	88.01	77.92	71.2	90.79	74.67	65.96	86.67	60.52	54.65	64.17
		Ours	**94.75**	**92.32**	**90.21**	**91.71**	**89.21**	**93.00**	**94.67**	**93.32**	**91.61**	**90.52**	**90.72**	**91.79**

based on graph hubness propagation model is effective, and can characterize the dynamic evolution of brain networks. Ours5 does not extract spatio-temporal features collaborative, so its performance is inferior to the proposed method, which also proves the importance of MCST-GCN in extracting spatio-temporal features.

In addition, we explore the influence of temporal attention mechanism (TA) and spatial attention mechanism (SA) on brain disease diagnosis. Specifically, we keep the same experimental settings and only consider whether TA or SA is added, and the experimental results are shown in Table V. As can be seen from Table V, if both TA and SA are not used, the classification accuracy will be greatly reduced. Adding either TA or SA will enhance the experimental results, and the performance is optimal when both of them are utilized. This indicates that our proposed SA and TA are able to focus on the spatio-temporal features related to brain diseases, thereby improving the disease diagnosis performance.

D. Discriminative Brain Connectivity and Regions

The spatio-temporal properties of brain networks can show the differences between healthy group and patient group, which has a significant role in disease diagnosis [3], [4]. Under such case, we compare the hubness propagation variability of different groups on two datasets. We obtain the average HOTENs based on each group and calculate the sum of variances of hubness propagation between brain regions to measure the information propagation variability. For the epilepsy dataset, the hubness propagation variability of NC, TLE and FLE are 0.846, 1.095 and 0.994, respectively. For the ADNI dataset, the hubness propagation variability of NC, SMC and EMCI are 0.667, 6.579 and 2.609, respectively. We can find that both epilepsy and cognitive impairment lead to more significant changes in hubness propagation between brain regions, while healthy people have more stable hubness propagation.

We investigate the effectiveness of the proposed method in identifying discriminative high-order brain connectivity associated with epilepsy. We evaluate the discriminative power of brain connectivities and regions using non-negative elastic networks [52]. Specifically, we employ the non-negative elastic network to establish a regression model from HOTENs to their corresponding diagnosis labels. These regression coefficients obtained in above model represent the significant alteration of each connectivity between patient group and healthy group. Then we rank the connectivities according to the values of their representation coefficients to find the discriminative brain connectivities. In addition, the discriminative power of each brain region is obtained by summing the regression coefficients of the connectivities associated with the corresponding brain region. We locate the 25 most discriminative brain connectivity from HOTENs by significant alteration of connectivity (SAC) [52] and visualize them in figure 7. For example, in NC vs. TLE, discriminative connections are mainly distributed in the Temporal pole: middle temporal gyrus, Inferior temporal gyrus and Hippocampus.L and these regions are closely related to memory function [53], [54]. The occurrence of TLE can lead to memory impairment, which indicates that these discriminative brain connections can distinguish NC from TLE to some extent. For NC vs FLE, key connections are mainly located in

TABLE III

THE CLASSIFICATION RESULT OF THE PROPOSED METHOD AND DIFFERENT BRAIN NETWORK FEATURE EXTRACTION METHODS (%)

Dataset	Modality	Method	NC vs. TLE&FLE			NC vs. TLE			NC vs. FLE			TLE vs. FLE		
			ACC	F1	AUC	ACC	F1	AUC	ACC	F1	AUC	ACC	F1	AUC
Epilepsy	DTI	BrainnetCNN [41]	64.08	77.37	76.22	69.83	56.77	76.37	66.93	65.11	71.08	60.00	55.56	55.21
		GCNN [42]	66.68	75.16	57.59	67.31	57.97	64.26	68.66	54.68	59.11	55.79	58.12	54.74
		MNC-Net [43]	73.19	79.86	63.25	70.36	53.49	65.43	67.32	60.01	61.14	66.68	56.35	57.34
	fMRI	GraphSAGE [26]	73.19	80.80	64.39	70.37	56.31	62.81	73.27	64.91	65.77	65.55	65.36	63.34
		SAGPool [44]	75.00	80.80	69.58	74.46	56.62	66.59	70.95	66.36	65.53	67.16	69.18	64.02
		CGRL [45]	76.91	80.41	67.31	74.00	55.58	64.95	73.37	69.15	61.20	68.16	65.95	58.75
		FE-STGNN [46]	72.84	78.69	64.18	72.81	70.68	68.31	76.75	55.60	61.90	68.74	64.42	55.56
		ST-fMRI [23]	76.18	83.26	70.58	71.79	53.53	69.39	72.84	67.02	72.68	68.79	62.77	63.06
	DTI &fMRI	GAT [47]	75.87	82.75	73.16	71.29	62.37	69.58	71.52	68.30	69.97	63.50	63.63	68.04
		AM-GCN [48]	75.54	81.07	71.67	75.21	60.31	74.36	74.70	71.05	70.63	66.74	66.38	61.40
		M-GCN [49]	77.42	83.72	67.32	75.00	61.53	58.70	78.33	68.29	69.38	65.00	66.67	61.84
		SCP-GCN [50]	78.75	80.00	65.16	71.67	60.47	59.06	72.98	54.39	68.08	65.56	62.86	62.23
		ST-GCN [51]	75.58	76.58	71.23	75.71	60.08	71.17	76.06	70.59	69.52	69.76	70.84	66.58
		STAGIN [24]	76.46	83.54	71.50	77.67	66.65	76.45	76.97	71.19	69.80	68.18	69.56	60.53
		Ours	**81.05**	**85.54**	**80.79**	**80.21**	**76.73**	**78.14**	**81.56**	**73.70**	**81.27**	**71.92**	**71.27**	**69.51**
Dataset	Modality	Method	NC vs. SMC&EMCI			NC vs. SMC			NC vs. EMCI			SMC vs. EMCI		
			ACC	F1	AUC	ACC	F1	AUC	ACC	F1	AUC	ACC	F1	AUC
ADNI	DTI	BrainnetCNN [41]	79.41	84.09	84.52	77.08	79.25	85.42	84.44	84.44	90.87	79.55	80.00	84.92
		GCNN [42]	86.30	89.92	81.06	86.67	83.47	77.82	86.68	70.23	83.92	84.23	82.89	85.07
		MNC-Net [43]	79.19	85.42	81.80	82.83	80.61	86.80	75.33	69.13	67.57	72.38	74.03	71.18
	fMRI	GraphSAGE [26]	86.70	89.42	89.48	89.21	87.49	90.28	91.33	90.58	**91.74**	78.48	71.97	74.35
		SAGPool [44]	77.27	85.71	62.50	74.54	61.40	65.21	73.33	71.43	69.64	71.43	83.33	66.25
		CGRL [45]	83.43	80.82	83.58	85.62	86.23	86.42	84.86	79.90	83.46	82.76	78.56	80.82
		FE-STGNN [46]	82.61	88.23	87.50	81.25	84.21	82.54	80.00	80.00	81.48	78.57	80.00	83.67
		ST-fMRI [23]	86.25	89.36	88.98	87.92	85.39	87.73	88.04	86.74	88.72	82.00	81.28	82.23
	DTI &fMRI	GAT [47]	86.26	88.91	84.54	89.29	86.90	91.42	86.67	81.75	86.47	78.48	79.22	79.89
		AM-GCN [48]	89.43	91.60	89.62	87.50	75.00	76.36	88.67	85.21	86.08	78.57	85.71	86.67
		M-GCN [49]	88.04	90.08	88.34	88.63	87.51	92.06	90.00	84.16	86.77	79.71	77.48	79.40
		SCP-GCN [50]	87.17	89.24	89.20	86.16	86.12	84.94	84.67	76.19	84.48	79.90	79.13	81.78
		ST-GCN [51]	87.63	89.88	84.17	87.33	85.52	85.38	86.00	76.17	84.91	81.29	82.70	81.29
		STAGIN [24]	91.30	88.89	**90.77**	87.42	85.46	87.67	85.33	82.79	85.97	82.05	79.14	75.59
		Ours	**94.75**	**92.32**	90.21	**91.71**	**89.21**	**93.00**	**94.67**	**93.32**	91.61	**90.52**	**90.72**	**91.79**

TABLE IV

THE RESULTS OF ABLATION EXPERIMENTS ON DIFFERENT TASKS (%)

Dataset	Method	Dynamic networks	Optimal transport	MCST-GCN	NC vs. TLE&FLE			NC vs. TLE			NC vs. FLE			TLE vs. FLE		
					ACC	F1	AUC	ACC	F1	AUC	ACC	F1	AUC	ACC	F1	AUC
Epilepsy	Ours1				73.50	79.52	68.44	71.43	66.67	67.27	76.36	69.50	73.20	63.94	64.66	59.23
	Ours2	✓			76.25	77.10	66.83	78.13	64.11	64.77	75.00	59.05	67.82	68.50	63.69	61.55
	Ours3		✓		74.14	78.88	63.55	74.55	63.48	71.02	72.25	56.03	60.51	65.17	67.05	53.88
	Ours4			✓	77.76	81.53	76.83	75.02	70.64	73.79	73.75	60.88	67.21	67.66	58.02	59.54
	Ours5	✓	✓		79.33	79.55	58.75	79.09	75.64	76.06	77.00	61.58	66.11	70.34	63.65	60.27
	Ours6	✓		✓	77.37	83.27	75.36	78.00	68.39	68.73	75.00	70.59	75.76	58.31	62.60	58.36
	Ours7		✓	✓	78.00	78.33	58.18	78.50	56.18	63.21	79.75	70.79	77.40	64.58	61.02	61.08
	Ours	✓	✓	✓	**81.05**	**85.54**	**80.79**	**80.21**	**76.73**	**78.14**	**81.56**	**73.70**	**81.27**	**71.92**	**71.27**	**69.51**
					NC vs. SMC&EMCI			NC vs. SMC			NC vs. EMCI			SMC vs. EMCI		
ADNI	Ours1				84.09	86.23	89.81	86.75	85.14	90.58	88.00	84.44	91.48	73.52	73.29	64.94
	Ours2	✓			85.81	87.94	82.35	88.04	86.61	90.84	88.67	80.48	90.44	77.76	79.88	78.71
	Ours3		✓		88.93	90.96	89.63	89.92	**89.44**	91.91	89.33	83.45	90.00	87.52	87.80	83.90
	Ours4			✓	88.06	90.30	88.06	89.88	88.46	92.96	88.67	88.50	90.75	86.05	84.46	85.61
	Ours5	✓	✓		89.41	91.23	89.01	90.50	88.95	90.32	93.33	87.76	91.00	88.24	87.22	88.00
	Ours6	✓		✓	88.06	89.79	89.84	91.13	88.63	89.95	88.67	84.95	87.06	83.47	83.27	79.15
	Ours7		✓	✓	88.91	91.02	**90.58**	90.50	88.81	90.43	92.00	87.28	91.52	84.00	83.15	85.20
	Ours	✓	✓	✓	**94.75**	**92.32**	90.21	**91.71**	89.21	**93.00**	**94.67**	**93.32**	**91.61**	**90.52**	**90.72**	**91.79**

the precentral gyrus, middle frontal gyrus and inferior frontal gyrus in the frontal lobes. These brain regions are responsible for coordinated message processing and transport necessary for advanced cognition [55], [56], and cognitive dysfunction is the dominant manifestation of FLE, which proves that these brain connections may indeed be different between NC and

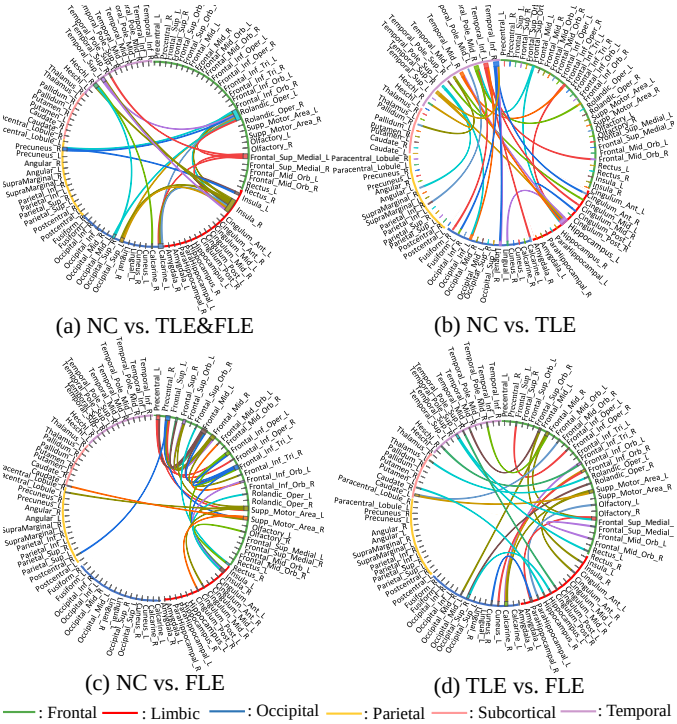

Fig. 7. The top 25 most key brain connections from HOTENs on different diagnosis tasks.

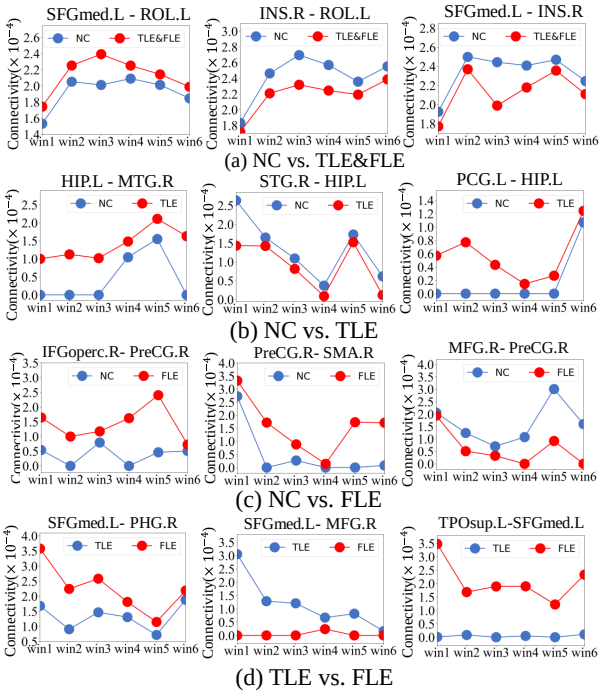

Fig. 8. The average values of the top 3 most discriminative dynamic connections of different groups on the four diagnosis tasks.

FLE patients. In addition, for NC vs. TLE&FLE, the identified SACs from HOTENs are mainly concentrated in regions such as Rolandic operculum, Insula, and Superior temporal gyrus. SACs in TLE vs. FLE are mainly distributed in the middle frontal gyrus, supplementary motor area and hippocampus, which have been shown to be closely related to epilepsy [53], [57], [58].

From figure 7, we can find that some discriminative brain connectivities are located in regions beyond the frontal and temporal lobes. For example, for the task of NC vs. TLE&FLE, the discriminative brain connectivities include Heschl.R-Insula.R, Occipital.Sub.L-Insula.R, Rolandic.Oper.L-Precuneus.R, etc. For the task of NC vs. TLE, the discriminative brain connectivities include Palidum.R-Temporal.Mid.L, Fusiform.R-Temporal.Pole.Mid.L, etc. For the task of NC vs. FLE, the discriminative brain connectivities include Postcentral.R-Precentral.R, Paracentral.Lobule.R-Supp.Motor.Area.L, etc. For the task of TLE vs. FLE, the discriminative brain connectivities include Occipital.Sub.R-Hippocampus.L, Caudate.L-Supp.Motor.Area.L, etc. This phenomenon could arise from the propagation of abnormal neural electrical activity due to epilepsy as well as compensatory mechanisms [59], [60]. Specifically, epilepsy is typically associated with abnormal electrical activity of neurons, which can be propagated to non-focal areas (such as Hippocampus, Insul, etc.) along with the information transmission between brain regions. In addition, epilepsy patients usually exhibit structural and functional abnormalities in the frontal and temporal regions. These irregularities can prompt other areas of the brain to undertake supplementary functions, compensating for the deficits in the affected regions.

To further reveal the changing patterns of brain network connectivity between different groups, we show the evolution

TABLE V

THE DIAGNOSIS ACCURACY OF ABLATION STUDY ON SPATIAL FEATURES ATTENTION AND TEMPORAL ATTENTION (%)

Method	NC vs.TLE & FLE	NC vs. TLE	NC vs. FLE	FLE vs. TLE
w/o SA+TA	79.35	78.00	75.73	66.73
w/o SA	79.81	78.75	76.75	67.18
w/o TA	80.89	80.25	78.71	69.84
Ours	**81.05**	**80.21**	**81.27**	**71.92**

w/o means without.

of the three most important SACs on the four classification tasks in figure 8, respectively. As shown in figure 8, there are significant differences in SACs between the different groups, so the discriminative connectivity in HOTENs can be used as a biomarker for the diagnosis of epilepsy and its subtypes. For example, in NC vs. TLE, HIP.L-MTG.R, and PCG.L-HIP.L show stronger connectivity strength in TLE than thats in NC. STG.R-HIP.L shows weaker connectivity strength in TLE than thats in NC. TLE is a long-term memory disorder disease, and Hippocampus controls human memory function [54]. Therefore, it is reasonable to use these connections as biomarkers for the diagnosis of TLE. In addition, such strong and weak patterns of key connections are also observed in the other three tasks. The analysis shows that our proposed HOTENs may help to find epilepsy related biomarkers and better understand the pathological mechanism of epilepsy.

We also investigate the top 10 most important brain regions from the HOTENs on different classification tasks and visualize them in figure 9. For example, the key brain regions of NC vs. TLE mainly include Inferior temporal gyrus, Hippocampus and middle temporal gyrus, etc., which are closely related to memory, and studies have shown that these brain regions play an important role in epilepsy diagnosis [61]. Therefore, we can task these brain regions as biomarkers to distinguish

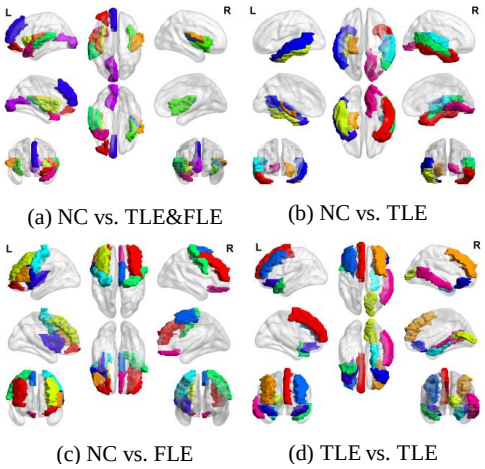

(a) NC vs. TLE&FLE (b) NC vs. TLE

(c) NC vs. FLE (d) TLE vs. TLE

Fig. 9. Distribution locations of the 10 most discriminative brain regions on different classification tasks.

NC from epilepsy patients. In the other three tasks, key brain regions include Temporal.Sup.L, Supplementary motor area, Precental gyrus, etc., which have been proven to be useful for recognizing epilepsy and its subtypes [53], [57], [58]. These experiments show that our method can provide effective biomarkers for epilepsy diagnosis.

E. Computational Efficiency Analysis

To investigate the computational efficiency of the model, we compare the quantities of model parameters (#Param) and floating-point operations (FLOPs) of the proposed method and several spatio-temporal feature extraction methods, including ST-fMRI, ST-GCN and STAGIN, shown in Table VI. As can be seen from Table VI, the proposed method has 4.14 million model parameters and involves 6.97 million FLOPs. Our method achieves the lowest FLOPs among all the spatio-temporal models, which indicates that our method requires less computational resources. Although our method has a slightly larger number of parameters than other spatio-temporal models, it achieves the best classification performance.

TABLE VI
COMPUTATIONAL EFFICIENCY OF THE PROPOSED METHOD AND OTHER SPATIO-TEMPORAL FEATURE EXTRACTION METHODS

Method	#Param (M)	FLOPs (M)
ST-fMRI	2.99	1045.02
ST-GCN	2.40	13.30
STAGIN	1.06	96.50
Ours	4.14	6.97

VI. Conclusion

In this paper, we propose a spatio-temporal graph structure propagation model to capture the topology evolutionary features in dynamic brain networks, It not only captures the network topology structure evolution information across the entire duration of the dynamic brain networks, but also effectively identifies discriminative spatio-temporal topology features for diagnosing brain diseases. First, we adaptively measure the graph hubness of each brain region of the brain network within each sliding window, which helps characterizes the complex correlations among multiple brain regions. Second, we propose an optimal transport based network dynamics model that simulates the network topology evolution process between adjacent brain networks, leveraging the structural brain network as the transport cost. These two steps facilitate the discovery of high-order interactions among brain regions, both spatially and temporally. Then, we develop a spatio-temporal graph convolutional network with an attention mechanism to extract spatio-temporal features from the obtained high-order dynamic brain networks. Finally, we employ a multi-layer perceptron approach to categorize these extracted spatio-temporal features. The experimental results demonstrate that our method outperforms various state-of-the-art brain network analysis approaches in identify epilepsy and cognitive impairment. Moreover, our approach could identify robust spatio-temporal topological biomarkers that offer promising prospects for enhancing the diagnosis of brain disorders.

References

[1] J. M. Shine, "The thalamus integrates the macrosystems of the brain to facilitate complex, adaptive brain network dynamics," *Progress in Neurobiology*, vol. 199, p. 101951, 2021.

[2] Y. Yang, H. Cui, and C. Yang, "Pre-train graph neural networks for brain network analysis," in *2022 IEEE International Conference on Big Data*, pp. 4993–4994.

[3] E. Christiaen, M.-G. Goossens, R. Raedt, B. Descamps, L. E. Larsen, E. Craey, E. Carrette, K. Vonck, P. Boon, and C. Vanhove, "Alterations in the functional brain network in a rat model of epileptogenesis: A longitudinal resting state fmri study," *Neuroimage*, vol. 202, p. 116144, 2019.

[4] J. Zhang, L. Zhou, L. Wang, M. Liu, and D. Shen, "Diffusion kernel attention network for brain disorder classification," *IEEE Transactions on Medical Imaging*, vol. 41, no. 10, pp. 2814–2827, 2022.

[5] Y. Long, H. Cao, C. Yan, X. Chen, L. Li, F. X. Castellanos, T. Bai, Q. Bo, G. Chen, N. Chen *et al.*, "Altered resting-state dynamic functional brain networks in major depressive disorder: Findings from the rest-meta-mdd consortium," *NeuroImage: Clinical*, vol. 26, p. 102163, 2020.

[6] Y. Yang, C. Ye, X. Guo, T. Wu, Y. Xiang, and T. Ma, "Mapping multi-modal brain connectome for brain disorder diagnosis via cross-modal mutual learning," *IEEE Transactions on Medical Imaging*, pp. 1–14, 2023, DOI: 10.1109/TMI.2023.3294967.

[7] H. Zhang, R. Song, L. Wang, L. Zhang, D. Wang, C. Wang, and W. Zhang, "Classification of brain disorders in rs-fmri via local-to-global graph neural networks," *IEEE Transactions on Medical Imaging*, vol. 42, no. 2, pp. 444–455, 2022.

[8] H. Ju and D. S. Bassett, "Dynamic representations in networked neural systems," *Nature Neuroscience*, vol. 23, no. 8, pp. 908–917, 2020.

[9] J. Liu, X. Liao, M. Xia, and Y. He, "Chronnectome fingerprinting: Identifying individuals and predicting higher cognitive functions using dynamic brain connectivity patterns," *Human Brain Mapping*, vol. 39, no. 2, pp. 902–915, 2018.

[10] B. Jie, M. Liu, and D. Shen, "Integration of temporal and spatial properties of dynamic connectivity networks for automatic diagnosis of brain disease," *Medical Image Analysis*, vol. 47, pp. 81–94, 2018.

[11] F. Noman, S.-Y. Yap, R. C.-W. Phan, H. Ombao, and C.-M. Ting, "Graph autoencoder-based embedded learning in dynamic brain networks for autism spectrum disorder identification," in *2022 IEEE International Conference on Image Processing (ICIP)*, 2022, pp. 2891–2895.

[12] A. Zou, J. Ji, M. Lei, J. Liu, and Y. Song, "Exploring brain effective connectivity networks through spatiotemporal graph convolutional models," *IEEE Transactions on Neural Networks and Learning Systems*, pp. 1–13, 2022, DOI: 10.1109/TNNLS.2022.3221617.

[13] H. Y. Chiu, L. Zhao, and A. Wu, "Jgat: a joint spatio-temporal graph attention model for brain decoding," *arXiv preprint arXiv:2306.05286*, 2023.

[14] H. Huang, Q. Liu, Y. Jiang, Q. Yang, X. Zhu, and Y. Li, "Deep spatio-temporal attention-based recurrent network from dynamic adaptive functional connectivity for mci identification," *IEEE Transactions on Neural Systems and Rehabilitation Engineering*, vol. 30, pp. 2600–2612, 2022.

[15] L. Liu, G. Wen, P. Cao, T. Hong, J. Yang, X. Zhang, and O. R. Zaiane, "Braintgl: A dynamic graph representation learning model for brain network analysis," *Computers in Biology and Medicine*, vol. 153, p. 106521, 2023.

[16] Q. Zhang, B. Guo, W. Kong, X. Xi, Y. Zhou, and F. Gao, "Tensor-based dynamic brain functional network for motor imagery classification," *Biomedical Signal Processing and Control*, vol. 69, p. 102940, 2021.

[17] M. Perrot, N. Courty, R. Flamary, and A. Habrard, "Mapping estimation for discrete optimal transport," *Advances in Neural Information Processing Systems*, vol. 29, 2016.

[18] F. Tong and M. S. Pratte, "Decoding patterns of human brain activity," *Annual Review of Psychology*, vol. 63, pp. 483–509, 2012.

[19] X. Wang, D. Jiao, X. Zhang, and X. Lin, "Altered degree centrality in childhood absence epilepsy: a resting-state fmri study," *Journal of the Neurological Sciences*, vol. 373, pp. 274–279, 2017.

[20] K. Song, J. Li, Y. Zhu, F. Ren, L. Cao, and Z.-G. Huang, "Altered small-world functional network topology in patients with optic neuritis: A resting-state fmri study," *Disease Markers*, vol. 2021, 2021.

[21] T. Watanabe and G. Rees, "Brain network dynamics in high-functioning individuals with autism," *Nature Communications*, vol. 8, no. 1, p. 16048, 2017.

[22] G. Zhang, B. Cai, A. Zhang, J. M. Stephen, T. W. Wilson, V. D. Calhoun, and Y.-P. Wang, "Estimating dynamic functional brain connectivity with a sparse hidden markov model," *IEEE Transactions on Medical Imaging*, vol. 39, no. 2, pp. 488–498, 2019.

[23] S. Dahan, L. Z. Williams, D. Rueckert, and E. C. Robinson, "Improving phenotype prediction using long-range spatio-temporal dynamics of functional connectivity," in *Machine Learning in Clinical Neuroimaging: 4th International Workshop, MLCN 2021, Held in Conjunction with MICCAI 2021, Strasbourg, France, September 27, 2021, Proceedings 4*. Springer, 2021, pp. 145–154.

[24] B.-H. Kim, J. C. Ye, and J.-J. Kim, "Learning dynamic graph representation of brain connectome with spatio-temporal attention," *Advances in Neural Information Processing Systems*, vol. 34, pp. 4314–4327, 2021.

[25] B. Yu, H. Yin, and Z. Zhu, "Spatio-temporal graph convolutional networks: A deep learning framework for traffic forecasting," *arXiv preprint arXiv:1709.04875*, 2017.

[26] W. Hamilton, Z. Ying, and J. Leskovec, "Inductive representation learning on large graphs," *Advances in neural information processing systems*, vol. 30, 2017.

[27] Z. Qin, Z. Liu, and P. Zhu, "Aiding alzheimer's disease diagnosis using graph convolutional networks based on rs-fmri data," in *2022 15th International Congress on Image and Signal Processing, BioMedical Engineering and Informatics (CISP-BMEI)*, pp. 1–7.

[28] T. N. Kipf and M. Welling, "Semi-supervised classification with graph convolutional networks," *arXiv preprint arXiv:1609.02907*, 2016.

[29] S. I. Ktena, S. Parisot, E. Ferrante, M. Rajchl, M. Lee, B. Glocker, and D. Rueckert, "Metric learning with spectral graph convolutions on brain connectivity networks," *NeuroImage*, vol. 169, pp. 431–442, 2018.

[30] J. Hauke and T. Kossowski, "Comparison of values of pearson's and spearman's correlation coefficients on the same sets of data," *Quaestiones geographicae*, vol. 30, no. 2, pp. 87–93, 2011.

[31] M. A. Al-Garadi, K. D. Varathan, S. D. Ravana, E. Ahmed, G. Mujtaba, M. U. S. Khan, and S. U. Khan, "Analysis of online social network connections for identification of influential users: Survey and open research issues," *ACM Computing Surveys (CSUR)*, vol. 51, no. 1, pp. 1–37, 2018.

[32] M. Cuturi, "Sinkhorn distances: Lightspeed computation of optimal transport," *Advances in Neural Information Processing Systems*, vol. 26, 2013.

[33] L. Qiao, H. Zhang, M. Kim, S. Teng, L. Zhang, and D. Shen, "Estimating functional brain networks by incorporating a modularity prior," *Neuroimage*, vol. 141, pp. 399–407, 2016.

[34] X. Kan, H. Cui, J. Lukemire, Y. Guo, and C. Yang, "Fbnetgen: Task-aware gnn-based fmri analysis via functional brain network generation," in *International Conference on Medical Imaging with Deep Learning*. PMLR, 2022, pp. 618–637.

[35] Q. Zhu, J. Zhu, M. Liu, X. Xu, and D. Zhang, "Multi-region correlation based functional brain network for disease diagnosis and cognitive states detection," *IEEE Access*, vol. 6, pp. 78 065–78 076, 2018.

[36] H. Zhang, X. Chen, Y. Zhang, and D. Shen, "Test-retest reliability of "high-order" functional connectivity in young healthy adults," *Frontiers in Neuroscience*, vol. 11, p. 439, 2017.

[37] S. S. Menon and K. Krishnamurthy, "A comparison of static and dynamic functional connectivities for identifying subjects and biological sex using intrinsic individual brain connectivity," *Scientific reports*, vol. 9, no. 1, p. 5729, 2019.

[38] X. Chen, H. Zhang, Y. Gao, C.-Y. Wee, G. Li, D. Shen, and A. D. N. Initiative, "High-order resting-state functional connectivity network for mci classification," *Human Brain Mapping*, vol. 37, no. 9, pp. 3282–3296, 2016.

[39] F. Zhao, Z. Chen, I. Rekik, S.-W. Lee, and D. Shen, "Diagnosis of autism spectrum disorder using central-moment features from low-and high-order dynamic resting-state functional connectivity networks," *Frontiers in Neuroscience*, vol. 14, p. 258, 2020.

[40] Y. Zhang, H. Zhang, X. Chen, S.-W. Lee, and D. Shen, "Hybrid high-order functional connectivity networks using resting-state functional mri for mild cognitive impairment diagnosis," *Scientific reports*, vol. 7, no. 1, p. 6530, 2017.

[41] J. Kawahara, C. J. Brown, S. P. Miller, B. G. Booth, V. Chau, R. E. Grunau, J. G. Zwicker, and G. Hamarneh, "Brainnetcnn: Convolutional neural networks for brain networks; towards predicting neurodevelopment," *NeuroImage*, vol. 146, pp. 1038–1049, 2017.

[42] T.-A. Song, S. R. Chowdhury, F. Yang, H. Jacobs, G. El Fakhri, Q. Li, K. Johnson, and J. Dutta, "Graph convolutional neural networks for alzheimer's disease classification," in *IEEE 16th International Symposium on Biomedical Imaging (ISBI 2019)*, 2019, pp. 414–417.

[43] L. Huang, X. Ye, M. Yang, L. Pan, and S. hua Zheng, "Mnc-net: Multi-task graph structure learning based on node clustering for early parkinson's disease diagnosis," *Computers in Biology and Medicine*, vol. 152, p. 106308, 2023.

[44] J. Lee, I. Lee, and J. Kang, "Self-attention graph pooling," in *International Conference on Machine Learning*. PMLR, 2019, pp. 3734–3743.

[45] R. Hu, L. Peng, J. Gan, X. Shi, and X. Zhu, "Complementary graph representation learning for functional neuroimaging identification," in *Proceedings of the 30th ACM International Conference on Multimedia*, 2022, pp. 3385–3393.

[46] D. Chen and L. Zhang, "Fe-stgnn: Spatio-temporal graph neural network with functional and effective connectivity fusion for mci diagnosis," in *International Conference on Medical Image Computing and Computer-Assisted Intervention*. Springer, 2023, pp. 67–76.

[47] P. Veličković, G. Cucurull, A. Casanova, A. Romero, P. Lio, and Y. Bengio, "Graph attention networks," *arXiv preprint arXiv:1710.10903*, 2017.

[48] X. Wang, M. Zhu, D. Bo, P. Cui, C. Shi, and J. Pei, "Am-gcn: Adaptive multi-channel graph convolutional networks," in *Proceedings of the 26th ACM SIGKDD International Conference on Knowledge Discovery & Data Mining*, 2020, pp. 1243–1253.

[49] N. S. Dsouza, M. B. Nebel, D. Crocetti, J. Robinson, S. Mostofsky, and A. Venkataraman, "M-gcn: A multimodal graph convolutional network to integrate functional and structural connectomics data to predict multidimensional phenotypic characterizations," in *Medical Imaging with Deep Learning*. PMLR, 2021, pp. 119–130.

[50] J. Liu, G. Ma, F. Jiang, C.-T. Lu, S. Y. Philip, and A. B. Ragin, "Community-preserving graph convolutions for structural and functional joint embedding of brain networks," in *IEEE International Conference on Big Data*, 2019, pp. 1163–1168.

[51] S. Gadgil, Q. Zhao, A. Pfefferbaum, E. V. Sullivan, E. Adeli, and K. M. Pohl, "Spatio-temporal graph convolution for resting-state fmri analysis," in *Medical Image Computing and Computer Assisted Intervention–MICCAI 2020: 23rd International Conference, Lima, Peru, October 4–8, 2020, Proceedings, Part VII 23*. Springer, 2020, pp. 528–538.

[52] Q. Zhu, J. Huang, and X. Xu, "Non-negative discriminative brain functional connectivity for identifying schizophrenia on resting-state fmri," *Biomedical Engineering Online*, vol. 17, no. 1, pp. 1–15, 2018.

[53] M. K. Alvim, A. C. Coan, B. M. Campos, C. L. Yasuda, M. C. Oliveira, M. E. Morita, and F. Cendes, "Progression of gray matter atrophy in seizure-free patients with temporal lobe epilepsy," *Epilepsia*, vol. 57, no. 4, pp. 621–629, 2016.

[54] M. P. Richardson, B. A. Strange, J. S. Duncan, and R. J. Dolan, "Preserved verbal memory function in left medial temporal pathology involves reorganisation of function to right medial temporal lobe," *Neuroimage*, vol. 20, pp. S112–S119, 2003.

[55] W. Liu, Q. Yue, Q. Gong, D. Zhou, and X. Wu, "Regional and remote connectivity patterns in focal extratemporal lobe epilepsy," *Annals of Translational Medicine*, vol. 9, no. 14, 2021.

[56] P. Liang, Z. Wang, Y. Yang, and K. Li, "Three subsystems of the inferior parietal cortex are differently affected in mild cognitive impairment," *Journal of Alzheimer's Disease*, vol. 30, no. 3, pp. 475–487, 2012.

[57] E. Widjaja, S. Z. Mahmoodabadi, O. C. Snead III, A. Almehdar, and M. L. Smith, "Widespread cortical thinning in children with frontal lobe epilepsy," *Epilepsia*, vol. 52, no. 9, pp. 1685–1691, 2011.

[58] S. Vulliemoz, C. Vollmar, M. J. Koepp, M. Yogarajah, J. O'Muircheartaigh, D. W. Carmichael, J. Stretton, M. P. Richardson, M. R. Symms, and J. S. Duncan, "Connectivity of the supplementary

motor area in juvenile myoclonic epilepsy and frontal lobe epilepsy," *Epilepsia*, vol. 52, no. 3, pp. 507–514, 2011.

[59] M. Mariam Bee and K. Vidhya, "A detailed survey on epilepsy detection using the classifications of eeg signals," in *Emerging Technologies in Data Mining and Information Security: Proceedings of IEMIS 2020, Volume 3*. Springer, 2021, pp. 555–562.

[60] G. Bettus, E. Guedj, F. Joyeux, S. Confort-Gouny, E. Soulier, V. Laguitton, P. J. Cozzone, P. Chauvel, J.-P. Ranjeva, F. Bartolomei *et al.*, "Decreased basal fmri functional connectivity in epileptogenic networks and contralateral compensatory mechanisms," *Human brain mapping*, vol. 30, no. 5, pp. 1580–1591, 2009.

[61] S. G. Mueller, K. D. Laxer, J. Barakos, I. Cheong, P. Garcia, and M. W. Weiner, "Widespread neocortical abnormalities in temporal lobe epilepsy with and without mesial sclerosis," *Neuroimage*, vol. 46, no. 2, pp. 353–359, 2009.